ACS APPLIED NANO MATERIALS

www.acsanm.org Article

Mild Liquid-Phase Exfoliation of Transition Metal Dichalcogenide Nanosheets for Hydrogen Evolution

Jian Zhang, Tianyu Ji, Huihui Jin,* Zhe Wang, Ming Zhao, Daping He, Guoqiang Luo, and Boyang Mao*

Cite This: *ACS Appl. Nano Mater.* 2022, 5, 8020−8028 Read Online

ACCESS | Metrics & More | Article Recommendations | Supporting Information

ABSTRACT: Developing a general strategy to efficiently exfoliate transition metal dichalcogenide (TMD) electrocatalysts would be significantly beneficial for the electrocatalytic hydrogen evolution reaction (HER) from water splitting. However, there are several challenges in the production of two-dimensional (2D) TMDs, including the complicated fabrication process, high defect rate, and low production yield. Herein, we developed a general applicable mild organic molecular intercalator-assisted liquid-phase exfoliation method to produce TMD nanosheets in a large scale. The as-prepared ultrathin WSe_2, $MoSe_2$, WS_2, and MoS_2 nanosheets have a 2D nanosheet structure with a thickness of ∼3 nm and lateral size in a few hundred nanometers. This mild intercalation method can avoid introducing harsh exfoliation conditions used in conventional liquid-phase exfoliation, electrochemistry exfoliation, and lithium intercalation, thus resulting in high-quality exfoliation of TMD crystals. Additionally, benefiting from superior intrinsic electrical conductivity, unique 2D structure, and highly exposed active sites, the exfoliated WSe_2 and $MoSe_2$ nanosheets exhibited excellent catalytic activity for HER in acid with overpotentials of 223 and 225 mV at a current density of 10 mA cm^{-2} and low Tafel slopes of 64 and 65 mV dec^{-1}, respectively.

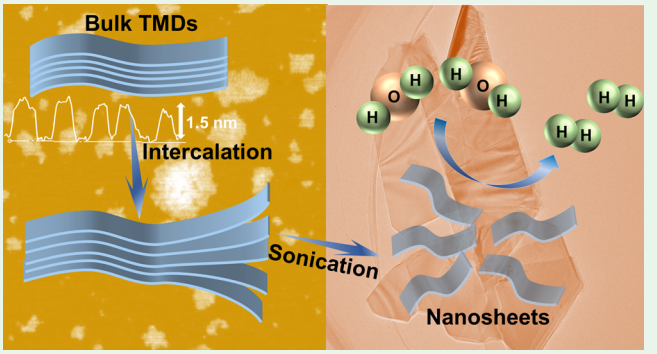

KEYWORDS: *transition metal dichalcogenides, hydrogen evolution reaction, two-dimensional materials, liquid-phase exfoliation, intercalation*

INTRODUCTION

The development of hydrogen energy is one of the best ways to maintain sustainable development and address environmental pollution issue and energy crisis.[1−3] At present, the commercial catalysts for hydrogen evolution reaction (HER) are dominated by precious metals (Pt, Ru, Pd, etc.), but the shortage of resources and the instability of precious metals severely limit the development of hydrogen energy.[4,5] Among the numerous non-precious metal HER catalysts, transition metal dichalcogenides (TMDs) have attracted extensive attention because their free energy of hydrogen adsorption (ΔG_H) is closer to the thermoneutral value and they have a low material cost, so they are expected to be a good alternative to precious metal commercial HER catalysts.[6−8] Bulk layered TMDs widely exist in nature; however, their catalytical properties are severely limited due to the insufficiency of edge active sites.[9] Accordingly, the preparation of ultrathin, exfoliated two-dimensional (2D) TMDs to release a larger specific surface area and more edge active sites is the key to advance TMDs in HER applications.[10,11] Up to now, two strategies have been applied to produce 2D TMD nanosheets, including bottom-up and top-down.[12,13] Chemical vapor deposition and physical vapor deposition are two common bottom-up methods for producing large-area and high-quality TMDs, but the relatively complexed experimental conditions (such as high temperatures of 600−1000 °C, vacuum environment, and so on) and difficulty in transferring onto a substrate significantly increase the cost, making these two methods more suitable for electronic applications rather than industry-scale catalyst applications.[14,15] For the top-down approach, it mainly contains mechanical cleavage and liquid-phase exfoliation (LPE). Although mechanical cleavage can be used to obtain high-quality single-layer TMD,[16,17] the production is limited. LPE is a well-studied, convenient, and facile approach to produce mass scale 2D-TMD materials; however, conventional LPE normally results in poor-quality TMDs, requiring prolonged production time, and limited by low exfoliation rate.[18,19]

Received: March 15, 2022
Accepted: May 3, 2022
Published: June 2, 2022

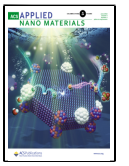

https://doi.org/10.1021/acsanm.2c01136
ACS Appl. Nano Mater. 2022, 5, 8020−8028

In recent years, electrochemical exfoliation and intercalation-assisted LPE have been intensively investigated and developed to improve the quality and efficiency of LPE exfoliation. Electrochemical exfoliation employs an electric current as a driving force to intercalate large size intercalators into layered materials, resulting in successful exfoliation with high exfoliation yield and good exfoliation quality.[20,21] However, electrochemical exfoliation requires the raw bulk materials to be conductive and in large dimension single crystals to work as an electrode.[22] Large voltages and high temperatures are also required for certain plasma-induced electrochemical exfoliation.[13] Intercalation-assisted exfoliation is usually driven by chemical heat to insert alkali metal ions or molecules into the free spacing of the TMD layers to produce nanosheets.[23] For example, lithium intercalation-assisted exfoliation is one of the well-studied intercalation methods to exfoliate 2D layered materials.[24] However, lithium is highly explosive and sensitive to oxygen and water, which makes it unsafe in mass production.[25,26] In addition, such methods are relatively ineffective for selenides and tellurides.[27] As a result, finding a mild intercalation agent to further promote the development of intercalation-assisted exfoliation is critical.

Herein, we produced ultrathin TMDs nanosheets using a mild intercalation-assisted liquid exfoliation strategy. In this study, driven by thermal dynamics, dodecyl trimethyl ammonium chloride is used as a general intercalant to intercalate into TMD materials. To demonstrate its general applicability, four TMD materials are investigated in this paper: WSe_2, $MoSe_2$, WS_2, and MoS_2. Full morphology and structure characterizations show that bulk WSe_2, $MoSe_2$, WS_2, and MoS_2 can be successfully exfoliated into single or few layer nanosheets after intercalation with an ultrathin thickness of ~3 nm and contain less defects. The lateral sizes of the four exfoliated nanosheets are around 500 nm or below. Compared with conventional LPE which uses prolonged time sonication, our method requires less ultrasonic time and is feasible for sensitive layered materials, which is applicable for sulfide and also effective for selenides. Moreover, although layered MoS_2 and WS_2 have been shown to be effective in HER electrocatalysts, WSe_2 and $MoSe_2$ have better electrical conductivity, making them preferable to sulfide in HER.[28] In this study, we investigated four exfoliated TMD nanosheets but focused on testing the performance of WSe_2 and $MoSe_2$. Benefiting from their unique 2D structure and highly exposed active sites, the exfoliated WSe_2 and $MoSe_2$ nanosheets exhibited excellent catalytic activity for the HER in acid with overpotentials of 223 and 225 mV at a current density of 10 mA cm^{-2} and low Tafel slopes of 64 and 65 mV dec^{-1}, respectively.[29] Among them, the performance of WSe_2 is superior to those reported for other WSe_2-based HER electrocatalysts.

EXPERIMENTAL SECTION

Synthesis of Exfoliated TMDs. The exfoliated TMDs were produced by intercalation-assisted LPE. The synthesis mechanism of exfoliated TMDs is shown in Figure 1a. First, 0.25 g of bulk TMD powder (99.999%, Six Carbon Technology, Shenzhen) was mixed with 1.5 g of dodecyl trimethylammonium chloride (99%, Aladdin) in 125 mL of dimethyl sulfoxide (DMSO) (99.8%, Aladdin). The reaction was performed for 48 h under the protection of N_2 at 160 °C. The intercalated mixture was repeatedly washed with ethanol to remove DMSO from the surface, and then, 35 mL of *N*-methyl-2-pyrrolidone (NMP) (99.5%, Aladdin) was added for use. The exfoliation was carried out with an ultrasonicator (Ultrasonic Processor 300 W, Cole-Parmer, amplitude 20%) with a probe tip for 30 min using a cyclic program of 3 s on followed by 2 s off. Subsequently, the exfoliated TMDs were collected via centrifugation at 1500 rpm for 15 min. The prepared nanosheet dispersion solution was vacuum-dried at 65 °C for 10 h to obtain the final powder.

Electrochemical Measurements. All electrochemical measurements were performed on a CHI760E electrochemical workstation (Chenhua, Shanghai), in which a glassy carbon (GC) electrode (3 mm in diameter, 0.07 cm^2) with catalyst ink acted as the working electrode in a standard three-electrode cell system, a graphite rod was used as the counter electrode, and a saturated calomel electrode (SCE) was used as the reference electrode. The electrochemical HER measurements were performed in 0.5 M H_2SO_4 solutions at 25 °C. Prior to the test, the surface of the GC electrode was polished with 0.05 μm alumina particles on a polishing pad and then rinsed with deionized water and dried, and N_2 gas was injected for 30 min to remove oxygen from the electrolyte. Typically, 2.5 mg of catalyst and 2.5 mg of XC-72 with 50 μL of Nafion solution (5 wt %) were dispersed in 450 μL of ethanol and treated with ultrasound for 30 min to form a uniform ink. Next, uniform ink is loaded onto the surface of the GC electrode (loading amount of 0.357 mg cm^{-2}). Linear sweep voltammetry was carried out from −0.2 to −0.65 V (vs SCE) with a scan rate of 5 mV s^{-1}. All polarization curves were presented with *iR* correction. The formula for compensation is as follows: E (correction) = E (measurement) − iR, where i is the measured current and R is obtained from the impedance test of the corresponding material. All the potentials were converted into the reversible hydrogen electrode (RHE) reference scale by using the Nernst equation: $E_{(\text{vs RHE})} = E_{(\text{vs SCE})} + 0.0591 \times \text{pH} + 0.244$ V. To investigate the long-term stability of exfoliated TMDs, cyclic voltammetry (CV) was carried out in a potential window of −0.5 to −0.4 V (vs SCE) at a sweep rate of 50 mV s^{-1}. Electrochemical impedance spectroscopy (EIS) was obtained at an overpotential of 0.48 V (vs SCE) with an amplitude of 5 mV and frequency range of $1-10^5$ Hz. CV was performed at different scanning rates (20−200 mV s^{-1}) in the potential range of −0.244 to −0.044 V (vs SCE) to estimate the electrochemically active surface area (ECSA).

Calculation Method. The present first-principles density functional theory (DFT) calculations are performed by Vienna Ab initio Simulation Package (VASP) with the projector augmented wave method.[30,31] The exchange-functional is treated using the generalized gradient approximation of the Perdew−Burke−Ernzerhof functional. The energy cutoff for the plane-wave basis expansion was set to 450 eV, and the force on each atom less than 0.02 eV/Å was set for the convergence criterion of geometry relaxation.[32] 15 Å vacuum was adopted for all systems in order to avoid the interaction between periodic structures. The Brillouin zone integration is performed using 1 × 3 × 1 or 3 × 1 × 1 for WSe_2 (-1010) or $MoSe_2$ (10-10), respectively. The self-consistent calculations apply a convergence energy threshold of 10^{-5} eV. The DFT-D3 method was employed to consider the van der Waals interaction.[33]

The Free energies of the adsorption atomic hydrogen (ΔG_H) was calculated by using equation[34]

$$\Delta G_H = \Delta E_{DFT} + \Delta E_{ZPE} - T\Delta S \quad (1)$$

where ΔE_{DFT} is the DFT energy difference and the ΔE_{ZPE} and $T\Delta S$ terms were obtained based on vibration analysis.

RESULTS AND DISCUSSION

The composition of layered TMD materials is MX_2, where M = transition metal and X = chalcogenides, such as S, Se, Te, and so forth. Each layer in TMDs is three atoms thick and made up of XMX, where the MX bonds are held together by strong covalent bonds and only weak van der Waals attraction exists between each stacking layer.[12] Figure S1 illustrates the single-layer and multilayer stacking structures of MX_2. Each layer of MX_2 is superimposed vertically along with the crystallization, and the weak van der Waals force is maintained

https://doi.org/10.1021/acsanm.2c01136
ACS Appl. Nano Mater. 2022, 5, 8020−8028

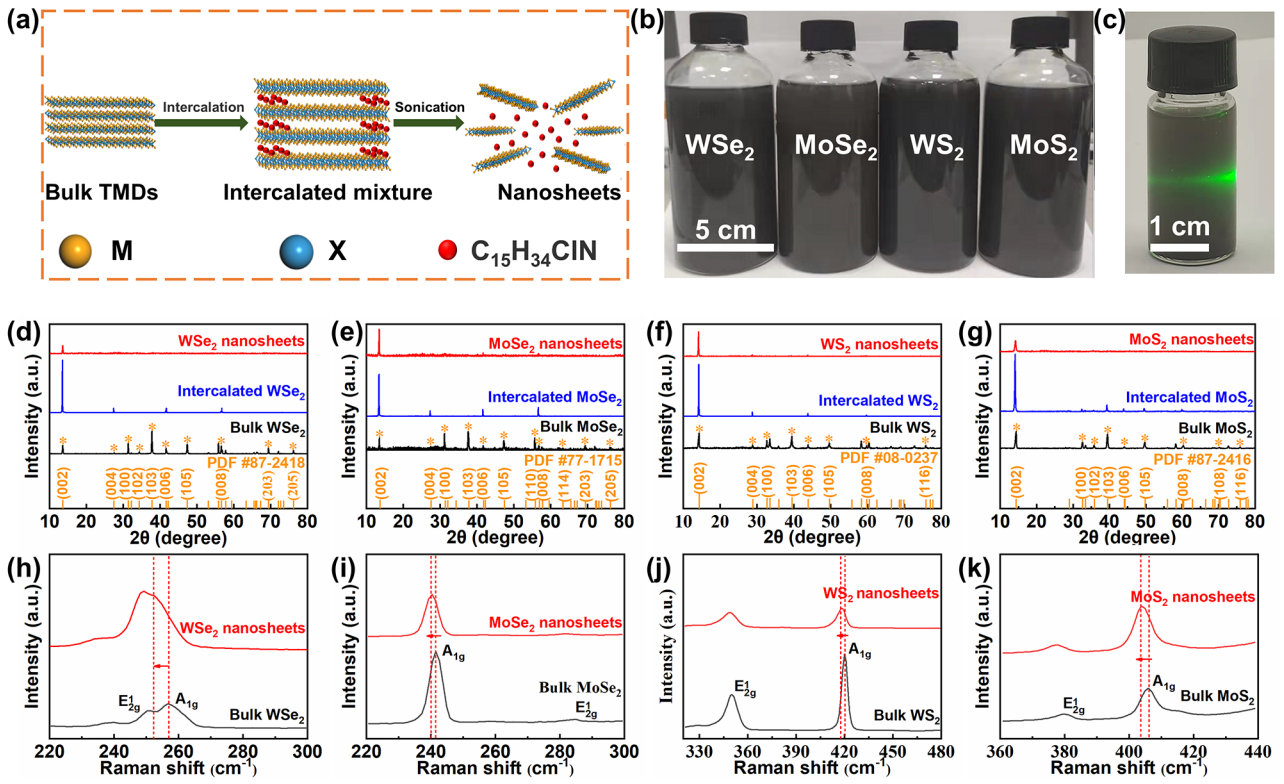

Figure 1. (a) Schematic of intercalation and exfoliation. Transition metal (M), chalcogenides (X), and dodecyl trimethyl ammonium chloride ($C_{15}H_{34}ClN$) are represented by orange, blue, and red balls, respectively. (b) Photographs of four exfoliated TMD nanosheets dispersed in NMP solvent. (c) Tyndall effect of the WSe_2 nanosheets after exfoliation. X-ray diffraction (XRD) patterns of (d) WSe_2, (e) $MoSe_2$, (f) WS_2, and (g) MoS_2. Raman spectra of (h) WSe_2, (i) $MoSe_2$, (j) WS_2, and (k) MoS_2.

between layers.[35,36] Figure 1a represents the mechanism of our intercalation-assisted LPE at where dodecyl trimethyl ammonium chloride molecules are thermally dynamically intercalated into the interlayer of raw bulk TMDs (powder) as a long chain molecule to expand the interlayer spacing and weaken the van der Waals attraction. Due to the extended free spacing and generated sheer force, TMDs can then be exfoliated in NMP with mild ultrasound in less than 30 min to obtain stable TMD suspensions (Figure 1b), which can exhibit a Tyndall effect, as shown in Figure 1c, indicating well-dispersed TMD nanosheets and successful exfoliation.

The XRD patterns of four bulk TMDs and their corresponding intercalation and exfoliation are shown in Figure 1d−g. The bulk TMDs' diffraction peaks are all consistent with their standard diffraction file.[37] All of the TMDs' (00*l*) peaks are enhanced after intercalation, while others are weakened or disappear. This trend is because during/after exfoliation, the nanosheets' structure reassembles in 00*l* reflect direction and forms a more ordered laminate structure rather than being randomly oriented in bulk materials. Furthermore, the positions of the magnified (002) peaks are shifted to the left (Figure S2), indicating that the layer spacing expands to some extent according to the Bragg equation $2d \sin \theta = n\lambda$.[38] All of the (002) peaks are more pronounced with ultrasound treatment, and almost all of the other peaks have vanished, indicating the success of TMD exfoliation.[10,39] Figure 1h,i shows the Raman spectrum of WSe_2 and $MoSe_2$, respectively. The bulk WSe_2 has two distinct strong peaks at 251 and 256 cm^{-1}, corresponding to the (in-plane) and A_{1g} (out-of-plane) modes,[40] while the two strong peaks of the bulk $MoSe_2$ are located at 241.6 and 284.1 cm^{-1}.[41] All of the full width at half-maximum of nanosheets' peaks is found to increase and A_{1g} modes' redshift supports the success of exfoliating.[42,43] The same trend can also be observed in WS_2 and MoS_2 (Figure 1j,k). Furthermore, UV−vis absorption spectra of the exfoliated nanosheets containing all signature peaks demonstrated the exfoliated nanosheets' high quality (Figure S3).[44] The peak positions of the four TMDs correspond to their 2H phase, indicating that no phase transition has taken place after exfoliation.[13]

The chemical composition and valence information of the bulk WSe_2 and $MoSe_2$ and their corresponding nanosheets were further characterized using X-ray photoelectron spectroscopy (XPS) to demonstrate the nanosheets' quality. WSe_2 and $MoSe_2$ were chosen for further investigation because not only their 2D structure is less studied but also they are less stable when compared to WS_2 and MoS_2, making exfoliation more difficult. As shown in Figure S4a,d, no new impurities were introduced except for oxygen. The weak oxidation peaks of WSe_2 and $MoSe_2$ nanosheets may mainly attributed to the ultrathin WSe_2 and $MoSe_2$ nanosheets, which can be oxidized during test conditions. For WSe_2 nanosheets, the high-resolution of the W 4f spectrum displays two apparent peaks at 32.5 and 34.6 eV (Figure S4b), which are attributed to W $4f_{5/2}$ and W $4f_{7/2}$, respectively.[45] In Figure S4c, the fitting peaks Se 3d are located at 54.8 and 55.7 eV, corresponding to Se $3d_{5/2}$ and Se $3d_{3/2}$, respectively, confirming the formation of Se^{2-}.[46,47] Figure S4e,f shows the Mo 3d and Se 3d spectra of $MoSe_2$, respectively. According to the data, the peaks of $MoSe_2$ nanosheets at 232.1 and 229.1 eV coincide with the binding

https://doi.org/10.1021/acsanm.2c01136
ACS Appl. Nano Mater. 2022, 5, 8020−8028

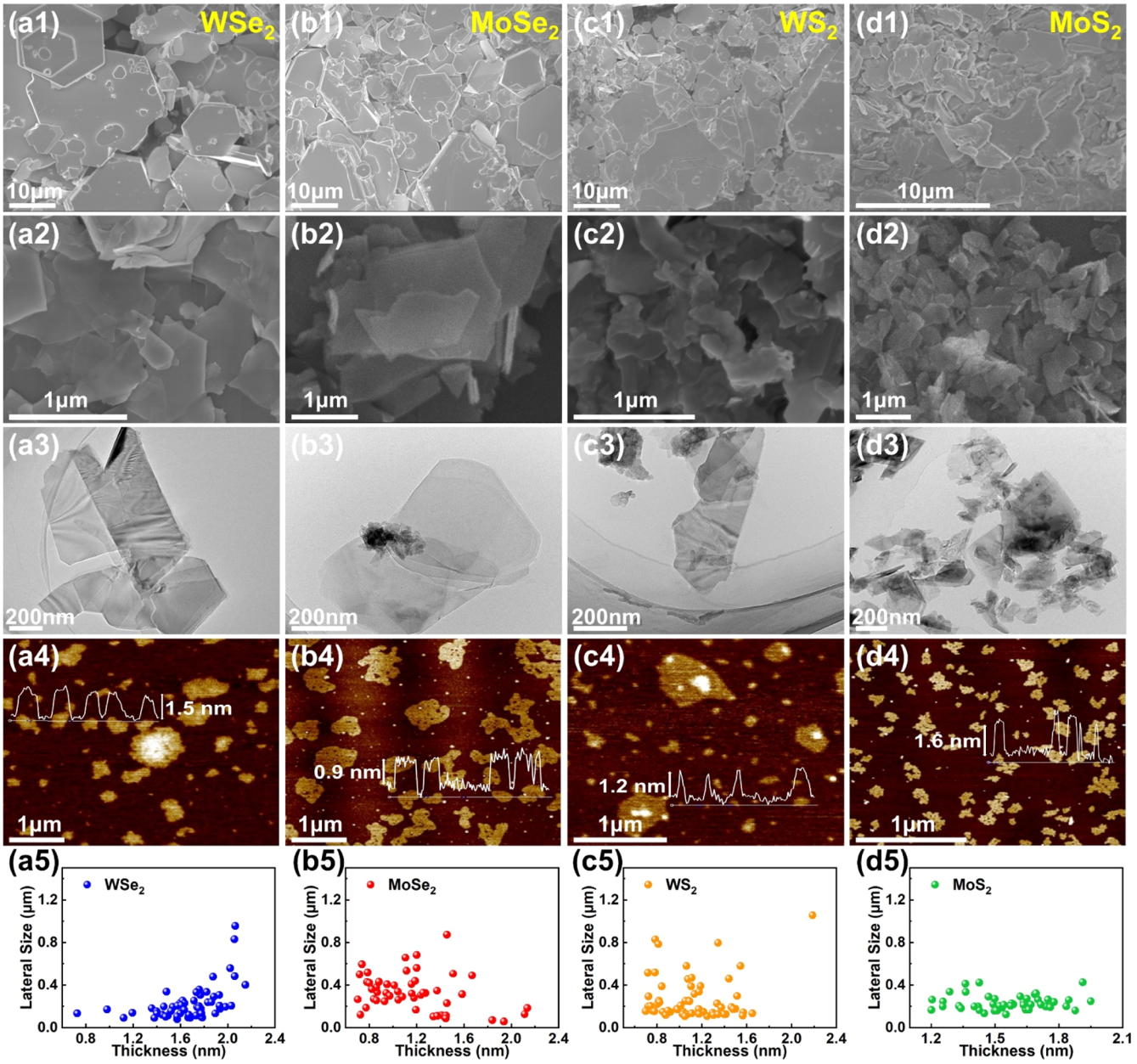

Figure 2. Scanning electron micrographs of bulk (a1) WSe_2, (b1) $MoSe_2$, (c1) WS_2, and (d1) MoS_2. Scanning electron micrographs of exfoliated (a2) WSe_2, (b2) $MoSe_2$, (c2) WS_2, and (d2) MoS_2 nanosheets. TEM images of exfoliated (a3) WSe_2, (b3) $MoSe_2$, (c3) WS_2, and (d3) MoS_2 nanosheets. AFM images of exfoliated (a4) WSe_2, (b4) $MoSe_2$, (c4) WS_2, and (d4) MoS_2 nanosheets. Statistical distribution of size and thickness of (a5) WSe_2, (b5) $MoSe_2$, (c5) WS_2, and (d5) MoS_2 nanosheets.

energies of Mo $3d_{3/2}$ and Mo $3d_{5/2}$, respectively, demonstrating that Mo is the +4 oxidation state. The high-resolution of Se 3d spectrum about $MoSe_2$ nanosheets show that its peaks are at 55.0 and 54.1 eV, corresponding to the Se $3d_{5/2}$ and Se $3d_{3/2}$, respectively.[48,49] The XPS results shown above demonstrate that no defects or impurities (such as organic intercalators or solvents residues) were introduced during the exfoliating process.

The morphology of the bulk raw materials and exfoliated samples were analyzed by scanning electron microscopy (SEM) and/or transmission electron microscopy (TEM). SEM images in Figures 2, S5, and S6 clearly show the morphological changes of WSe_2, $MoSe_2$, WS_2, and $MoSe_2$ during the exfoliation process. The bulk raw TMDs exhibit larger crystal sizes and thicknesses (Figure 2a1−d1). After intercalating with dodecyl trimethylammonium chloride, the outer edge of bulk TMDs is turned over, and the layer spacing is increased obviously. Even a small portion of the nanosheet is exfoliated successfully (Figures S5a,b and S6a,b). Furthermore, mild sonication reduces the thickness of exfoliated WSe_2, $MoSe_2$, WS_2, and $MoSe_2$ nanosheets, Figure 2a2−d2, and the lateral size is about and below 1 μm, and the morphology of corresponding individual nanosheets can be seen in Figures S5c,d and S6c,d. Figure 2a3−d3 shows the TEM images of exfoliated TMDs, which display super thin layers with clear boundary and complete crystal structure. Atomic force microscopy (AFM) images show that the thicknesses of exfoliated WSe_2, $MoSe_2$, WS_2, and $MoSe_2$ nanosheets are 1.5, 0.9, 1.2, and 1.6 nm, respectively, implying that the number of layers is about single layer or bilayer[33] (Figure 2a4−d4). Figure

https://doi.org/10.1021/acsanm.2c01136
ACS Appl. Nano Mater. 2022, 5, 8020−8028

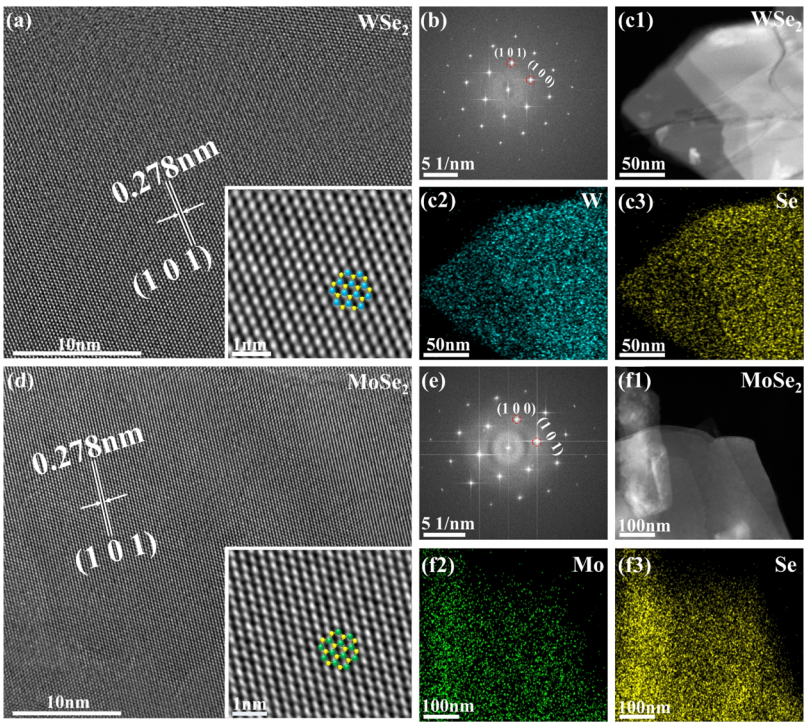

Figure 3. (a) HRTEM of WSe_2 nanosheets. Inset: its partial magnified image. Individual W and Se atoms forming the hexagonal structures were clearly observed, which are represented by green and yellow balls, respectively. (b) The corresponding FFT pattern. (c) EDX elemental mapping images of WSe_2 nanosheets. (d) HRTEM of $MoSe_2$ nanosheets. Inset: partial magnified image. Individual Mo and Se atoms forming the hexagonal structures were clearly observed, which are represented by green and yellow balls, respectively. (e) The corresponding FFT pattern. (f) EDX elemental mapping images of $MoSe_2$ nanosheets.

2a5−d5 further proves an ultrahigh yield of ∼100% of characterized 2D TMDs is at most three layers based on a statistical analysis of AFM images. To directly compare the advantages of thermal intercalation, we performed conventional LPE using only sonication to exfoliate bulk WSe_2 for 30 min, and the characterization results are shown in Figure S9. SEM images show that the lateral size of the WSe_2 nanosheets is about 1 μm. TEM and high-resolution TEM (HRTEM) show that the WSe_2 nanosheets have thick thickness and a large number of defects. AFM results confirm that the WSe_2 thickness obtained by direct liquid exfoliation is 47 nm, which is much higher than that obtained by intercalation-assisted liquid exfoliation.

To further assess the quality and thickness of exfoliated WSe_2 nanosheets, HRTEM was performed to analyze the crystal structure of exfoliated nanosheets. In Figure 3a,d, the lattice fringes of WSe_2 and $MoSe_2$ nanosheets are all measured to be 0.278 nm, corresponding to the (101) plane of the WSe_2 and (101) plane $MoSe_2$ crystal, respectively.[11] Insets in Figure 3a,d filtered the corresponding HRTEM images, revealing the continuous lattice fringes and periodic atomic arrangement of WSe_2 and $MoSe_2$ nanosheets, which also confirm their high crystallinity and hexagonal structure. Fast Fourier transform (FFT) of WSe_2 and $MoSe_2$ nanosheets demonstrate their hexagonal structure and well-stacked single-crystal layer feature (Figure 3b,e). Moreover, the uniform distribution of W, Mo, and Se elements in energy-dispersive X-ray spectroscopy (EDX) proves the excellent purity of WSe_2 nanosheets and $MoSe_2$ nanosheets (Figure 3c,f). Similarly, the exfoliating effects of WS_2 and MoS_2 are shown in Figures S7 and S8 exhibiting their high crystallinity and purity. These results suggest that the crystal structure of TMD nanosheets is not damaged significantly by intercalation and mild sonication.

Subsequently, the electrocatalytic performance of exfoliated TMD nanosheets was measured in 0.5 M H_2SO_4. As selenides have higher electrical conductivity than transition metal sulfides, we first explored the HER properties of WSe_2 and $MoSe_2$. Figure 4a,d shows the polarization curves of WSe_2 and $MoSe_2$, and all the potentials measured were *iR*-corrected. Due to the large specific surface area of the 2D structure,[50] the exfoliated WSe_2 and $MoSe_2$ nanosheets have overpotentials of 223 and 225 mV at the current density of 10 mA cm^{-2}, respectively, much lower than that of bulk WSe_2 (331 mV at 10 mA cm^{-2}) and $MoSe_2$ (291 mV at 10 mA cm^{-2}). To evaluate the electrochemical reaction kinetics involved in WSe_2 and $MoSe_2$, the Tafel slope was calculated by the Tafel formula: $\eta = b \log(j) + a$, where j is the current density and b is the Tafel slope. As shown in Figures S9a and S10a, the Tafel slope of the exfoliated WSe_2 and $MoSe_2$ nanosheets are 64 and 65 mV dec^{-1}, respectively, which are lower than bulk WSe_2 (82 mV dec^{-1}) and $MoSe_2$ (90 mV dec^{-1}). Based on the slope of the mechanism, the Volmer−Heyrovsky combinative mechanism may play a major role in the HER process of WSe_2 and $MoSe_2$ nanosheets.[13] Figures S9b and S10b give the comprehensive comparison of electrochemical properties. In Figures S9c and S10c, the polarization curve of WSe_2 and $MoSe_2$ nanosheets coincide before and after the CV test, indicating the robust stability of the catalyst. To further investigate the HER electron-transfer kinetics of WSe_2 and $MoSe_2$ nanosheets, EIS measurement was carried out at the potential of −0.236 V (vs RHE). Figure 4b,e shows the Nyquist plots of WSe_2 and $MoSe_2$ nanosheets fitted by an equivalent circuit with charge-transfer resistance (R_{ct}).$R_{ct}$is

https://doi.org/10.1021/acsanm.2c01136
ACS Appl. Nano Mater. 2022, 5, 8020−8028

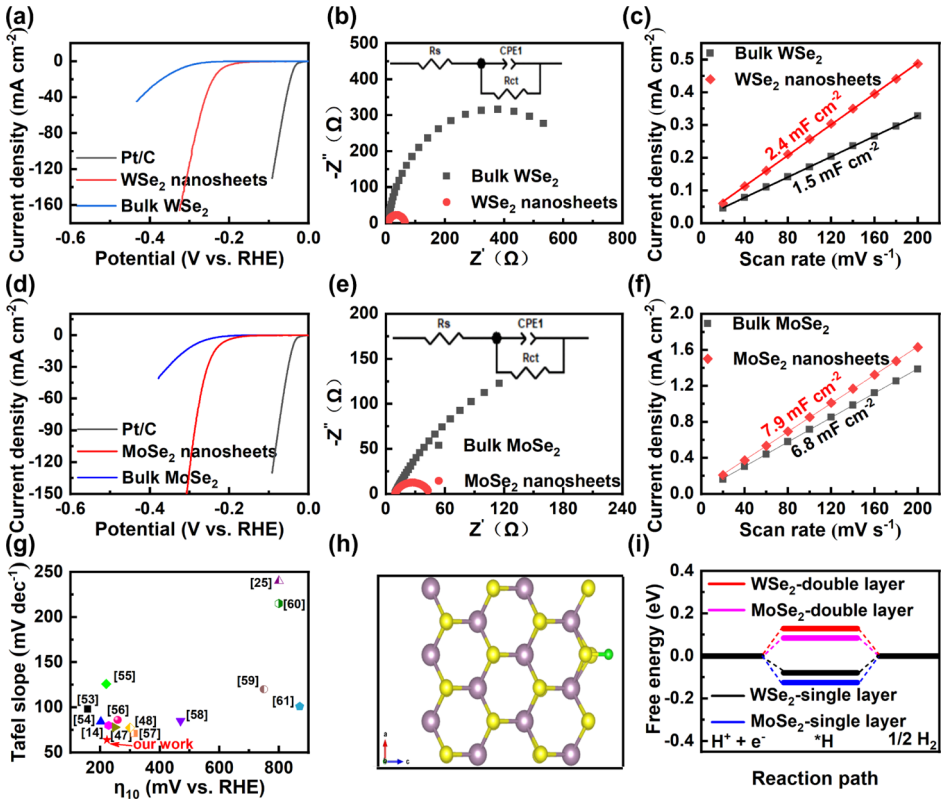

Figure 4. Polarization curves of (a) bulk WSe_2, WSe_2 nanosheets, and Pt/C, (d) bulk $MoSe_2$, $MoSe_2$ nanosheets, and Pt/C. Nyquist plots of (b) bulk WSe_2 and WSe_2 nanosheets, (e) bulk $MoSe_2$ and $MoSe_2$ nanosheets. Inset: an equivalent circuit for fitting impedance data. C_{dl} values of (c) bulk WSe_2 and WSe_2 nanosheets, (f) bulk $MoSe_2$ and $MoSe_2$ nanosheets. (g) Comparison of Tafel slope-η_{10} for WSe_2 nanosheets and WSe_2-based HER catalysts have been reported in other studies. (h) Scheme of the DFT models used for investigating WSe_2 and $MoSe_2$ catalytic activity, W/Mo, Se, and H_{ads} atoms are represented by purple, yellow, and green spheres, respectively. (i) Free energy vs the reaction coordinate of HER for WSe_2 and $MoSe_2$ nanosheets in different layers.

related to the charge-transfer process at the electrode interface. A low R_{ct} value indicates that the electron transfer rate and the reaction rate are faster.[51] Specific fitting results are given in Table S1. The R_{ct} values of WSe_2 and $MoSe_2$ nanosheets are 58.59 and 35.09 Ω, which are much lower than that of bulk WSe_2 (722.1 Ω) and bulk $MoSe_2$ (494.8 Ω). Besides, WSe_2 and $MoSe_2$ nanosheets have a much smaller radius of curvature than the bulk WSe_2 and $MoSe_2$, also revealing that the charge-transfer resistance of the nanosheet is minimal.[36] Additionally, C_{dl} was used to estimate the electrochemical active surface area of the catalyst,[52] and CV was performed at a sweep rate of 20−200 mV s^{-1} to calculate C_{dl} (Figure S11). The results show that the C_{dl} of WSe_2 nanosheets is 2.4 mF cm^{-2}, about 1.6 times larger than that of bulk WSe_2 (1.5 mF cm^{-2}), and the C_{dl} of $MoSe_2$ nanosheets is 7.9 mF cm^{-2}, about 1.2 times larger than that of bulk $MoSe_2$ (6.8 mF cm^{-2}) (Figure 4c,f). According to the results of EIS and ECSA, the exfoliated WSe_2 and $MoSe_2$ nanosheets both have better reaction kinetics and more active sites, which are attributed to the increase of specific surface area after exfoliation. In conclusion, the exfoliated WSe_2 and $MoSe_2$ nanosheets show excellent HER performance. Especially, the WSe_2 catalytic activity has exceeded most of the reported HER catalysts based on WSe_2 (Figure 4g).[14,25,47,48,53−61] It has been reported that by increasing specific surface area and doping, the HER performance of WSe_2 can be improved; however, many of the reported methods are complex to prepare, which highlights the advantages of our method. In order to reveal the origin of WSe_2 and $MoSe_2$ nanosheets' hydrogen evolution activities, DFT calculation was performed for the active surface of WSe_2 (-1010) and the active surface of $MoSe_2$ (10-10) (Figure 4h,i). According to the calculation results, the ΔG_H values of single-layer and double-layer WSe_2 nanosheets were −0.079 and 0.129, respectively, while those of $MoSe_2$ were −0.125 and 0.08, respectively (Table 1). As well known, low ΔG_H indicates

Table 1. Hydrogen Adsorption Free Energy Values of WSe_2 and $MoSe_2$ Nanosheets (ΔG_H)

surface condition	condition	ΔG_H
WSe_2 (-1010)	single-layer	−0.079
	double-layer	0.129
$MoSe_2$ (10-10)	single-layer	−0.125
	double-layer	0.08

strong bonding of H_{ads} and high ΔG_H indicates weak bonding of H_{ads} to catalyst surface, but both situations have a negative impact on HER dynamics.[62] An ideal catalyst should have the value of ΔG_H close to zero. According to the statistical results, our exfoliated WSe_2 and $MoSe_2$ nanosheets are concentrated in single and double layers, and their ΔG_H calculation results are very close to 0 eV, representing that the H_{ads} free energy is close to that of the reactant or product, which is an energetically feasible HER condition. The above calculation results strongly prove the improvement of HER performance after exfoliating. Finally, we explored HER performance of exfoliated WS_2 and MoS_2. In Figure S11a,d, the exfoliated WS_2

https://doi.org/10.1021/acsanm.2c01136
ACS Appl. Nano Mater. 2022, 5, 8020−8028

and MoS_2 nanosheets delivered overpotentials of 295 and 270 mV to reach the current density of 10 mA cm^{-2}, respectively, which was much lower than that of bulk WS_2 (376 mV at 10 mA cm^{-2}) and bulk MoS_2 (371 mV at 10 mA cm^{-2}). Figure S11b,e shows the Tafel curves of exfoliated WS_2 and MoS_2 nanosheets. After exfoliating, the Tafel slopes of WS_2 and MoS_2 decreased from 108 and 118 to 58 and 66 mV dec^{-1}, respectively. In Figure S11c,e, the polarization curve hardly attenuates after 1000 cycles, which proves the good stability of WS_2 and MoS_2 nanosheets.

CONCLUSIONS

In conclusion, we investigated a general, facile, novel solution-processable intercalation-assisted exfoliation method for preparing WSe_2, $MoSe_2$, WS_2, and MoS_2 nanosheets that has the potential to be extended to all other layered TMD materials. One of the benefits of our novel method is that it has few requirements for raw starting materials in terms of stability, crystal size, electrical conductivity, and so on. The characterization results confirmed that our exfoliated nanosheets are of high quality and with a single layer or bilayer ultrathin structure. The lateral sizes of the exfoliated nanosheets are in a few hundred nanometers. When exfoliated TMD nanosheets were used as electrocatalysts, they all performed among the best for HER under acidic conditions, especially WSe_2 and $MoSe_2$. Moreover, their superior performance was attributed primarily to their high crystallinity and more active sites exposed to the 2D structure, which was also confirmed by DFT calculations. Our results indicate that intercalation-assisted LPE of TMD nanosheets in HER is feasible and provides a simple and effective method for mass production of two-dimensional materials. This method is expected to be beneficial for preparing two-dimensional materials in other applications using intercalation-assisted LPE.

ASSOCIATED CONTENT

Supporting Information

The Supporting Information is available free of charge at https://pubs.acs.org/doi/10.1021/acsanm.2c01136.

Instrument for characterization; structure diagram of MX_2; XRD, Raman spectra, UV−vis spectra, SEM, EDS, and HRTEM data for the characterization of exfoliated MoS_2 and WS_2; SEM, UV−vis spectra, and XPS spectra of WSe_2 and $MoSe_2$; and electrochemical HER measurements (PDF)

AUTHOR INFORMATION

Corresponding Authors

Huihui Jin − *Hubei Engineering Research Center of RF-Microwave Technology and Application, School of Science, Wuhan University of Technology, Wuhan 430070, China*; Email: Jinhuihui@whut.edu.cn

Boyang Mao − *Department of Engineering, University of Cambridge, Cambridge CB3 0FA, U.K.*; orcid.org/0000-0001-8295-0090; Email: bm573@cam.ac.uk

Authors

Jian Zhang − *State Key Lab of Advanced Technology for Materials Synthesis and Processing, Wuhan University of Technology, Wuhan 430070, China*

Tianyu Ji − *State Key Lab of Advanced Technology for Materials Synthesis and Processing, Wuhan University of Technology, Wuhan 430070, China*; orcid.org/0000-0003-2150-979X

Zhe Wang − *Hubei Engineering Research Center of RF-Microwave Technology and Application, School of Science, Wuhan University of Technology, Wuhan 430070, China*; orcid.org/0000-0003-1412-8980

Ming Zhao − *Hubei Engineering Research Center of RF-Microwave Technology and Application, School of Science, Wuhan University of Technology, Wuhan 430070, China*

Daping He − *Hubei Engineering Research Center of RF-Microwave Technology and Application, School of Science, Wuhan University of Technology, Wuhan 430070, China*; orcid.org/0000-0002-0284-4990

Guoqiang Luo − *State Key Lab of Advanced Technology for Materials Synthesis and Processing, Wuhan University of Technology, Wuhan 430070, China*; orcid.org/0000-0001-7879-0012

Complete contact information is available at: https://pubs.acs.org/10.1021/acsanm.2c01136

Notes

The authors declare no competing financial interest.

ACKNOWLEDGMENTS

The authors gratefully acknowledge the financial support from the Guangdong Major Project of Basic and Applied Basic Research (Grant No. 2021B0301030001), the National Natural Science Foundation of China (Grant No. 52171045), and the major program of the specialized technological innovation of Hubei Province, China (Grant No. 2019AFA176).

REFERENCES

(1) Zhu, Q.; Qu, Y.; Liu, D.; Ng, K. W.; Pan, H. Two-Dimensional Layered Materials: High-Efficient Electrocatalysts for Hydrogen Evolution Reaction. *ACS Appl. Nano Mater.* **2020**, *3*, 6270−6296.

(2) Niu, S.; Cai, J.; Wang, G. Two-Dimensional MoS_2 for Hydrogen Evolution Reaction Catalysis: The Electronic Structure Regulation. *Nano Res.* **2021**, *14*, 1985−2002.

(3) Du, L.; Sun, Y.; You, B. Hybrid Water Electrolysis: Replacing Oxygen Evolution Reaction for Energy-Efficient Hydrogen Production and Beyond. *Mater. Reports Energy* **2021**, *1*, 100004.

(4) Su, J.; Liu, G.; Liu, L.; Chen, J.; Hu, X.; Li, Y.; Li, H.; Zhai, T. Recent Advances in 2D Group VB Transition Metal Chalcogenides. *Small* **2021**, *17*, 2005411.

(5) Hasani, A.; Tekalgne, M.; Le, Q. V.; Jang, H. W.; Kim, S. Y. Two-Dimensional Materials as Catalysts for Solar Fuels: Hydrogen Evolution Reaction and CO_2 Reduction. *J. Mater. Chem. A* **2019**, *7*, 430−454.

(6) Tsai, C.; Chan, K.; Abild-Pedersen, F.; Nørskov, J. K. Active Edge Sites in $MoSe_2$ and WSe_2 Catalysts for the Hydrogen Evolution Reaction: A Density Functional Study. *Phys. Chem. Chem. Phys.* **2014**, *16*, 13156−13164.

(7) Chhowalla, M.; Shin, H. S.; Eda, G.; Li, L.-J.; Loh, K. P.; Zhang, H. The Chemistry of Two-Dimensional Layered Transition Metal Dichalcogenide Nanosheets. *Nat. Chem.* **2013**, *5*, 263−275.

(8) Chia, X.; Pumera, M. Characteristics and Performance of Two-Dimensional Materials for Electrocatalysis. *Nat. Catal.* **2018**, *1*, 909−921.

(9) Zhu, J.; Wang, Z. C.; Dai, H.; Wang, Q.; Yang, R.; Yu, H.; Liao, M.; Zhang, J.; Chen, W.; Wei, Z.; Li, N.; Du, L.; Shi, D.; Wang, W.; Zhang, L.; Jiang, Y.; Zhang, G. Boundary Activated Hydrogen Evolution Reaction on Monolayer MoS_2. *Nat. Commun.* **2019**, *10*, 1348.

(10) Chen, H.; Si, J.; Lyu, S.; Zhang, T.; Li, Z.; Lei, C.; Lei, L.; Yuan, C.; Yang, B.; Gao, L.; Hou, Y. Highly Effective Electrochemical Exfoliation of Ultrathin Tantalum Disulfide Nanosheets for Energy-Efficient Hydrogen Evolution Electrocatalysis. *ACS Appl. Mater. Interfaces* **2020**, *12*, 24675−24682.
(11) Majidi, L.; Yasaei, P.; Warburton, R. E.; Fuladi, S.; Cavin, J.; Hu, X.; Hemmat, Z.; Cho, S. B.; Abbasi, P.; Vörös, M.; Cheng, L.; Sayahpour, B.; Bolotin, I. L.; Zapol, P.; Greeley, J.; Klie, R. F.; Mishra, R.; Khalili-Araghi, F.; Curtiss, L. A.; Salehi-Khojin, A. New Class of Electrocatalysts Based on 2D Transition Metal Dichalcogenides in Ionic Liquid. *Adv. Mater.* **2019**, *31*, 1804453.
(12) Samadi, M.; Sarikhani, N.; Zirak, M.; Zhang, H.; Zhang, H.-L.; Moshfegh, A. Z. Group 6 Transition Metal Dichalcogenide Nanomaterials: Synthesis, Applications and Future Perspectives. *Nanoscale Horiz.* **2018**, *3*, 90−204.
(13) Nguyen, V.-T.; Yang, T.-Y.; Le, P. A.; Yen, P.-J.; Chueh, Y.-L.; Wei, K.-H. New Simultaneous Exfoliation and Doping Process for Generating MX_2 Nanosheets for Electrocatalytic Hydrogen Evolution Reaction. *ACS Appl. Mater. Interfaces* **2019**, *11*, 14786−14795.
(14) Zou, M.; Zhang, J.; Zhu, H.; Du, M.; Wang, Q.; Zhang, M.; Zhang, X. A 3D Dendritic WSe_2 Catalyst Grown on Carbon Nanofiber Mats for Efficient Hydrogen Evolution. *J. Mater. Chem. A* **2015**, *3*, 12149−12153.
(15) Rajapakse, M.; Karki, B.; Abu, U. O.; Pishgar, S.; Musa, M. R. K.; Riyadh, S. M. S.; Yu, M.; Sumanasekera, G.; Jasinski, J. B. Intercalation as a Versatile Tool for Fabrication, Property Tuning, and Phase Transitions in 2D Materials. *npj 2D Mater. Appl.* **2021**, *5*, 30.
(16) Novoselov, K. S.; Geim, A. K.; Morozov, S. V.; Jiang, D.; Zhang, Y.; Dubonos, S. V.; Grigorieva, I. V.; Firsov, A. A. Electric Field in Atomically Thin Carbon Films. *Science* **2004**, *306*, 666−669.
(17) Oh, N. K.; Lee, H. J.; Choi, K.; Seo, J.; Kim, U.; Lee, J.; Choi, Y.; Jung, S.; Lee, J. H.; Shin, H. S.; Park, H. Nafion-Mediated Liquid-Phase Exfoliation of Transition Metal Dichalcogenides and Direct Application in Hydrogen Evolution Reaction. *Chem. Mater.* **2018**, *30*, 4658−4666.
(18) Hu, C.-X.; Shin, Y.; Read, O.; Casiraghi, C. Dispersant-Assisted Liquid-Phase Exfoliation of 2D Materials beyond Graphene. *Nanoscale* **2021**, *13*, 460−484.
(19) Coleman, J. N.; Lotya, M.; O'Neill, A.; Bergin, S. D.; King, P. J.; Khan, U.; Young, K.; Gaucher, A.; De, S.; Smith, R. J.; Shvets, I. V.; Arora, S. K.; Stanton, G.; Kim, H.-Y.; Lee, K.; Kim, G. T.; Duesberg, G. S.; Hallam, T.; Boland, J. J.; Wang, J. J.; Donegan, J. F.; Grunlan, J. C.; Moriarty, G.; Shmeliov, A.; Nicholls, R. J.; Perkins, J. M.; Grieveson, E. M.; Theuwissen, K.; McComb, D. W.; Nellist, P. D.; Nicolosi, V. Two-Dimensional Nanosheets Produced by Liquid Exfoliation of Layered Materials. *Science* **2011**, *331*, 568−571.
(20) Ambrosi, A.; Pumera, M. Electrochemical Exfoliation of MoS_2 Crystal for Hydrogen Electrogeneration. *Chem.—Eur. J.* **2018**, *24*, 18551−18555.
(21) Si, J.; Chen, H.; Lei, C.; Suo, Y.; Yang, B.; Zhang, Z.; Li, Z.; Lei, L.; Chen, J.; Hou, Y. Electrochemical Exfoliation of Ultrathin Ternary Molybdenum Sulfoselenide Nanosheets to Boost the Energy-Efficient Hydrogen Evolution Reaction. *Nanoscale* **2019**, *11*, 16200−16207.
(22) Yang, S.; Zhang, P.; Nia, A. S.; Feng, X. Emerging 2D Materials Produced via Electrochemistry. *Adv. Mater.* **2020**, *32*, 1907857.
(23) Zhang, Q.; Mei, L.; Cao, X.; Tang, Y.; Zeng, Z. Intercalation and Exfoliation Chemistries of Transition Metal Dichalcogenides. *J. Mater. Chem. A* **2020**, *8*, 15417−15444.
(24) Zeng, Z.; Sun, T.; Zhu, J.; Huang, X.; Yin, Z.; Lu, G.; Fan, Z.; Yan, Q.; Hng, H. H.; Zhang, H. An Effective Method for the Fabrication of Few-Layer-Thick Inorganic Nanosheets. *Angew. Chem. Int. Ed.* **2012**, *51*, 9052−9056.
(25) Ambrosi, A.; Sofer, Z.; Pumera, M. 2H→1T Phase Transition and Hydrogen Evolution Activity of MoS_2, $MoSe_2$, WS_2, and WSe_2 Strongly Depends on the MX_2 Composition. *Chem. Commun.* **2015**, *51*, 8450−8453.
(26) Zhang, H. Ultrathin Two-Dimensional Nanomaterials. *ACS Nano* **2015**, *9*, 9451−9469.
(27) O'Neill, A.; Khan, U.; Coleman, J. N. Preparation of High Concentration Dispersions of Exfoliated MoS_2 with Increased Flake Size. *Chem. Mater.* **2012**, *24*, 2414−2421.
(28) Feng, W.; Pang, W.; Xu, Y.; Guo, A.; Gao, X.; Qiu, X.; Chen, W. Transition Metal Selenides for Electrocatalytic Hydrogen Evolution Reaction. *ChemElectroChem* **2020**, *7*, 31−54.
(29) Zhu, Z.; Wan, S.; Zhao, Y.; Gu, Y.; Wang, Y.; Qin, Y.; Zhang, Z.; Ge, X.; Zhong, Q.; Bu, Y. Recent Advances in Bismuth-Based Multimetal Oxide Photocatalysts for Hydrogen Production from Water Splitting: Competitiveness, Challenges, and Future Perspectives. *Mater. Reports Energy* **2021**, *1*, 100019.
(30) Kresse, G.; Furthmüller, J. Efficiency of Ab-Initio Total Energy Calculations for Metals and Semiconductors Using a Plane-Wave Basis Set. *Comput. Mater. Sci.* **1996**, *6*, 15−50.
(31) Blöchl, P. E. Projector Augmented-Wave Method. *Phys. Rev. B: Condens. Matter Mater. Phys.* **1994**, *50*, 17953−17979.
(32) Perdew, J. P.; Chevary, J. A.; Vosko, S. H.; Jackson, K. A.; Pederson, M. R.; Singh, D. J.; Fiolhais, C. Erratum: Atoms, Molecules, Solids, and Surfaces: Applications of the Generalized Gradient Approximation for Exchange and Correlation. *Phys. Rev. B: Condens. Matter Mater. Phys.* **1993**, *48*, 4978.
(33) Grimme, S.; Antony, J.; Ehrlich, S.; Krieg, H. A Consistent and Accurate Ab Initio Parametrization of Density Functional Dispersion Correction (DFT-D) for the 94 Elements H-Pu. *J. Chem. Phys.* **2010**, *132*, 154104.
(34) Tang, Q.; Jiang, D.-e. Mechanism of Hydrogen Evolution Reaction on 1T-MoS_2 from First Principles. *ACS Catal.* **2016**, *6*, 4953−4961.
(35) Li, J.; Shen, J.; Ma, Z.; Wu, K. Thickness-Controlled Electronic Structure and Thermoelectric Performance of Ultrathin SnS_2 Nanosheets. *Sci. Rep.* **2017**, *7*, 8914.
(36) Si, J.; Zheng, Q.; Chen, H.; Lei, C.; Suo, Y.; Yang, B.; Zhang, Z.; Li, Z.; Lei, L.; Hou, Y.; Ostrikov, K. Scalable Production of Few-Layer Niobium Disulfide Nanosheetsvia Electrochemical Exfoliation for Energy-Efficient Hydrogen Evolution Reaction. *ACS Appl. Mater. Interfaces* **2019**, *11*, 13205−13213.
(37) Duphil, D.; Bastide, S.; Rouchaud, J. C.; Pastol, J. L.; Legendre, B.; Lévy-Clément, C. The Chemical Synthesis in Solution and Characterization of Transition Metal Dichalcogenide MX_2 (M = Mo, W; X = S, Se) Nanoparticles. *Nanotechnology* **2004**, *15*, 828−832.
(38) Yang, Q.; Su, Y.; Chi, C.; Cherian, C. T.; Huang, K.; Kravets, V. G.; Wang, F. C.; Zhang, J. C.; Pratt, A.; Grigorenko, A. N.; Guinea, F.; Geim, A. K.; Nair, R. R. Ultrathin Graphene-Based Membrane with Precise Molecular Sieving and Ultrafast Solvent Permeation. *Nat. Mater.* **2017**, *16*, 1198−1202.
(39) Bissett, M. A.; Worrall, S. D.; Kinloch, I. A.; Dryfe, R. A. W. Comparison of Two-Dimensional Transition Metal Dichalcogenides for Electrochemical Supercapacitors. *Electrochim. Acta* **2016**, *201*, 30−37.
(40) Iamprasertkun, P.; Hirunpinyopas, W.; Deerattrakul, V.; Sawangphruk, M.; Nualchimplee, C. Controlling the Flake Size of Bifunctional 2D WSe_2 nanosheets as Flexible Binders and Supercapacitor Materials. *Nanoscale Adv.* **2021**, *3*, 653−660.
(41) Toh, R. J.; Mayorga-Martinez, C. C.; Sofer, Z.; Pumera, M. $MoSe_2$ Nanolabels for Electrochemical Immunoassays. *Anal. Chem.* **2016**, *88*, 12204−12209.
(42) Iamprasertkun, P.; Hirunpinyopas, W.; Tripathi, A. M.; Bissett, M. A.; Dryfe, R. A. W. Electrochemical Intercalation of MoO_3-MoS_2 Composite Electrodes: Charge Storage Mechanism of Non-Hydrated Cations. *Electrochim. Acta* **2019**, *307*, 176−187.
(43) Zhao, W.; Ghorannevis, Z.; Amara, K. K.; Pang, J. R.; Toh, M.; Zhang, X.; Kloc, C.; Tan, P. H.; Eda, G. Lattice Dynamics in Mono- and Few-Layer Sheets of WS_2 and WSe_2. *Nanoscale* **2013**, *5*, 9677−9683.
(44) Yeon, C.; Yun, S. J.; Yang, J.; Youn, D.-H.; Lim, J. W. Na-Cation-Assisted Exfoliation of MX_2 (M = Mo, W; X = S, Se) Nanosheets in an Aqueous Medium with the Aid of a Polymeric Surfactant for Flexible Polymer-Nanocomposite Memory Applications. *Small* **2018**, *14*, 1702747.

https://doi.org/10.1021/acsanm.2c01136
ACS Appl. Nano Mater. 2022, 5, 8020−8028

(45) Liu, Z.; Zhao, H.; Li, N.; Zhang, Y.; Zhang, X.; Du, Y. Assembled 3D Electrocatalysts for Efficient Hydrogen Evolution: WSe_2 Layers Anchored on Graphene Sheets. *Inorg. Chem. Front.* **2016**, *3*, 313−319.
(46) Fang, D.; He, F.; Xie, J.; Xue, L. Calibration of Binding Energy Positions with C1s for XPS Results. *J. Wuhan Univ. Technol., Mater. Sci. Ed.* **2020**, *35*, 711−718.
(47) Wang, X.; Chen, Y.; Zheng, B.; Qi, F.; He, J.; Li, Q.; Li, P.; Zhang, W. Graphene-like WSe_2 nanosheets for Efficient and Stable Hydrogen Evolution. *J. Alloys Compd.* **2017**, *691*, 698−704.
(48) Xu, C.; Peng, S.; Tan, C.; Ang, H.; Tan, H.; Zhang, H.; Yan, Q. Ultrathin S-Doped $MoSe_2$ Nanosheets for Efficient Hydrogen Evolution. *J. Mater. Chem. A* **2014**, *2*, 5597−5601.
(49) Lu, J.; Carvalho, A.; Chan, X. K.; Liu, H.; Liu, B.; Tok, E. S.; Loh, K. P.; Castro Neto, A. H.; Sow, C. H. Atomic Healing of Defects in Transition Metal Dichalcogenides. *Nano Lett.* **2015**, *15*, 3524−3532.
(50) Cao, J.; Lei, C.; Yang, J.; Cheng, X.; Li, Z.; Yang, B.; Zhang, X.; Lei, L.; Hou, Y.; Ostrikov, K. An Ultrathin Cobalt-Based Zeolitic Imidazolate Framework Nanosheet Array with a Strong Synergistic Effect towards the Efficient Oxygen Evolution Reaction. *J. Mater. Chem. A* **2018**, *6*, 18877−18883.
(51) Hou, Y.; Qiu, M.; Nam, G.; Kim, M. G.; Zhang, T.; Liu, K.; Zhuang, X.; Cho, J.; Yuan, C.; Feng, X. Integrated Hierarchical Cobalt Sulfide/Nickel Selenide Hybrid Nanosheets as an Efficient Three-Dimensional Electrode for Electrochemical and Photoelectrochemical Water Splitting. *Nano Lett.* **2017**, *17*, 4202−4209.
(52) Vikraman, D.; Hussain, S.; Truong, L.; Karuppasamy, K.; Kim, H.-J.; Maiyalagan, T.; Chun, S.-H.; Jung, J.; Kim, H.-S. Fabrication of MoS_2/WSe_2 Heterostructures as Electrocatalyst for Enhanced Hydrogen Evolution Reaction. *Appl. Surf. Sci.* **2019**, *480*, 611−620.
(53) Zou, M.; Chen, J.; Xiao, L.; Zhu, H.; Yang, T.; Zhang, M.; Du, M. WSe_2 and $W(Se_xS_{1-x})_2$ Nanoflakes Grown on Carbon Nanofibers for the Electrocatalytic Hydrogen Evolution Reaction. *J. Mater. Chem. A* **2015**, *3*, 18090−18097.
(54) Kwak, I. H.; Kwon, I. S.; Lee, J. H.; Lim, Y. R.; Park, J. Chalcogen-Vacancy Group VI Transition Metal Dichalcogenide Nanosheets for Electrochemical and Photoelectrochemical Hydrogen Evolution. *J. Mater. Chem. C* **2021**, *9*, 101−109.
(55) Nam, J. H.; Jang, M. J.; Jang, H. Y.; Park, W.; Wang, X.; Choi, S. M.; Cho, B. Room-Temperature Sputtered Electrocatalyst WSe_2 Nanomaterials for Hydrogen Evolution Reaction. *J. Energy Chem.* **2020**, *47*, 107−111.
(56) Kadam, S. R.; Enyashin, A. N.; Houben, L.; Bar-Ziv, R.; Bar-Sadan, M. Ni-WSe_2 Nanostructures as Efficient Catalysts for Electrochemical Hydrogen Evolution Reaction (HER) in Acidic and Alkaline Media. *J. Mater. Chem. A* **2020**, *8*, 1403−1416.
(57) Xu, W.; Chai, K.; Jiang, Y.-w.; Mao, J.; Wang, J.; Zhang, P.; Shi, Y. 2D Single Crystal WSe_2 and $MoSe_2$ Nanomeshes with Quantifiable High Exposure of Layer Edges from 3D Mesoporous Silica Template. *ACS Appl. Mater. Interfaces* **2019**, *11*, 17670−17677.
(58) Li, J.; Liu, P.; Qu, Y.; Liao, T.; Xiang, B. WSe_2/RGO Hybrid Structure: A Stable and Efficient Catalyst for Hydrogen Evolution Reaction. *Int. J. Hydrogen Energy* **2018**, *43*, 2601−2609.
(59) Eng, A. Y. S.; Ambrosi, A.; Sofer, Z.; Šimek, P.; Pumera, M. Electrochemistry of Transition Metal Dichalcogenides: Strong Dependence on the Metal-to-Chalcogen Composition and Exfoliation Method. *ACS Nano* **2014**, *8*, 12185−12198.
(60) Tan, S. M.; Sofer, Z.; Luxa, J.; Pumera, M. Aromatic-Exfoliated Transition Metal Dichalcogenides: Implications for Inherent Electrochemistry and Hydrogen Evolution. *ACS Catal.* **2016**, *6*, 4594−4607.
(61) Mazánek, V.; Mayorga-Martinez, C. C.; Bouša, D.; Sofer, Z.; Pumera, M. WSe_2 Nanoparticles with Enhanced Hydrogen Evolution Reaction Prepared by Bipolar Electrochemistry: Application in Competitive Magneto-Immunoassay. *Nanoscale* **2018**, *10*, 23149−23156.
(62) Vilekar, S. A.; Fishtik, I.; Datta, R. Kinetics of the Hydrogen Electrode Reaction. *J. Electrochem. Soc.* **2010**, *157*, B1040.

https://doi.org/10.1021/acsanm.2c01136
ACS Appl. Nano Mater. 2022, 5, 8020−8028